TECHNICAL NOTE

JAAS
www.rsc.org/jaas

Interfacial effects during the analysis of multilayer metal coatings by radio-frequency glow discharge optical emission spectroscopy

Part 2.† Evaluation of depth resolution function and application to thin multilayer coatings

R. Escobar Galindo,* E. Forniés and J. M. Albella

Instituto de Ciencia de Materiales de Madrid (CSIC), E-28049 Cantoblanco, Madrid, Spain. E-mail: rescobar@icmm.csic.es; Fax: +34 91 372 06 23; Tel: +34 91 372 14 20 (ext. 304)

Received 23rd February 2005, Accepted 15th June 2005
First published as an Advance Article on the web 21st September 2005

The crater shape effects in GDOES depth profiling of multilayer metal coatings, with an individual thickness layer >500 nm, studied in the foregoing paper, have been extended to the case of thinner layers (layer thickness <150 nm). The analysis of 10 bilayers of 70 nm chromium and 150 nm titanium showed an increased degradation of the composition depth profiles. The continuous change in shape of the crater after each interface induces a higher mixing of the thin layers. Reducing the thickness of the individual layers added new features to the depth profiles, such as changes on the symmetry of the profiles probably due to a mixing or simultaneous detection of consecutive bilayers. Ultra-thin chromium layers of 2.5 and 5 nm, buried at different depths in a titanium matrix up to a thickness of 3 μm, were properly resolved both near the surface and deeply embedded in the matrix and used to evaluate the depth resolution function of the GDOES technique. The relative depth resolutions of all the interfaces were estimated showing a typical dependence with depth (z) of the type $z^{-0.6–0.7}$.

The depth resolution of rf-GDOES experiments is an important issue in extending its application to the analysis of thin multilayer coatings.[1–7] According to the Mixing, Roughness and Information depth (MRI) model,[8,9] the surface roughness is thought to be the main factor contributing to the loss of resolution in GDOES depth profiles. The analysis performed by Shimizu *et al.* of ultra-thin films <10 nm thick remarked the excellent depth resolution of GDOES for highly flat surfaces.[10–15] But, as was pointed out by Hoffmann *et al.*,[16] other GDOES-specific effects, in particular the shape of the sputtering crater, may disturb the depth resolution in multilayer systems.

In a previous paper,[17] we showed that three different effects, related to the particular crater shape (crater edge, re-sputtering from the crater wall and roughening of the crater bottom), may contribute to the interface broadening in multilayer systems (layer thickness >500 nm), thus affecting the depth resolution in GDOES experiments. In the present work, all these effects are taken into account in the analysis of thinner chromium and titanium multilayer systems (layer thickness <150 nm). In particular, when the thickness of the individual layers is of the same order or thinner than the crater shape features (*i.e.* edge depth) an enhancement of the mixing effects can be expected. In addition, the crater shape may strongly vary when crossing the successive layer interfaces, adopting a new combined profile. Finally, by further reducing the thickness of the deposited layers, we have evaluated the depth resolution function of the system. To this end, delta chromium markers (2.5 and 5 nm thick) have been buried at different depths in a titanium matrix. The sputtering rate effects on the depth resolution of the layers have been also assessed by swapping the metals in the multilayers and delta markers.

The deposition of metal layers and multilayers, typically made of alternating titanium and chromium films of different thickness, was performed in a conventional balanced magnetron sputtering system, as described in the foregoing paper.[17] Table 1 gives a summary of the coatings studied in this work. Other details of the deposition procedure can be found elsewhere.[18]

(a) Depth resolution in Ti–Cr thin multilayer coatings

In order to demonstrate the application of GDOES analysis to studying thin multilayer coatings, we have deposited a system consisting of 10 bilayers of 70 nm chromium and 150 nm titanium. The final thickness of the coatings was 2.2 μm as measured by profilometry. In Fig. 1 a cross-sectional TEM micrograph (JEOL 4000 EX/II at 400 kV) shows the first deposited Ti and Cr layers. The abrupt interfaces and the constant thickness of these first layers, close to the silicon substrate, can be observed. The roughness of the layers was found to increase for the subsequently deposited layers due to the PVD sputtering process.

The GDOES quantified profile of Fig. 2 perfectly reproduces the bilayer composition of the whole coating. However, there is a clear decrease in the height of both the titanium and chromium peaks up to a depth of about 1.0 μm (80 and 70% for titanium and chromium, respectively). After 1.0 μm, the Cr peaks keep decreasing down to a minimum of 65%, measured for the last Cr layer. Directly related to this decrease, there is a broadening of the layer thickness from 75 to 95 nm. On the other hand, the height of the Ti peaks saturates at 80% from 1.0 to 1.5 μm depth, and then starts increasing up to 85% from that depth until the interface with the silicon substrate. This increase coincides with the appearance of the silicon signal. As described in ref. 17, the detection of silicon, well in advance of the real Ti/Si interface, has to do with the erosion of the substrate by the well edge of the GDOES crater. Contrary to

† For Part 1 see ref. 17.

DOI: 10.1039/b502774h

Table 1 Description of the studied coating systems

Coating	Substrate	Thickness
Multilayers Cr/Ti	Silicon	10 × (70 nm Cr/150 nm Ti) 20 × (55 nm Cr/70 nm Ti) 10 × (70 nm Ti/150 nm Cr)
5 nm Cr in Ti matrix	Silicon Polished steel Unpolished steel	3 μm
2.5 nm Cr in Ti matrix	Silicon	3 μm
5 nm Ti in Cr matrix	Silicon	3 μm

chromium, the titanium layer thickness remains constant around 145 ± 3 nm (standard deviation) for the whole coating.

The variation of the alternate Cr and Ti signals in Fig. 2 can be explained in terms of depth resolution loss induced by crater effects, discussed in the foregoing paper. These effects are further accentuated, both by the differences in the sputtering rates of the adjacent metals and by the depth to which the interface is buried. In particular, for the case of a thinner layer, with thickness narrower than the rising and decaying tails of every layer profile, the signal maxima and minima corresponding to consecutive layers can never reach either the 100% top or 0% bottom values, respectively. Instead, the difference between the maxima and minima keeps decreasing as a result of the larger influence of the crater effects with depth. Moreover, there is a continuous change in the shape of the crater after crossing each interface.[19] But, contrary to the case of the thick multilayer coatings, this change in the crater form further causes the mixing of the narrower layers. In fact, the crater shape at any instant is supposed to have a combined profile of that corresponding to each individual metal.

The observed increase in maxima and minima of the Ti and Cr profiles beyond 1.5 μm depth is related to a lower surface roughness near the substrate interface. TEM observations have proved the existence of an induced roughening, typically found in the growth of coatings during the deposition process. The roughness of the very first layers deposited on the silicon substrate (*i.e.*, the last layer sputtered by GDOES) is lower than the last deposited layers (the near-surface layers). Thus, it seems that although there is an increasing GDOES induced roughening of the layers with depth, saturation inside the coating is compensated for by flatter layers close to the Si interface.

The above-described effects are magnified when the thickness of the layers is reduced (20 bilayers of 55 nm chromium and 70 nm titanium) as shown in Fig. 3. As in Fig. 2, a decrease is observed down to 65% for both the amplitude maxima of the titanium and chromium signals to a depth of 1.5 μm. The decrease of the Ti amplitude is more pronounced than that observed in Fig. 2, revealing a greater mixing of the narrower bilayers. After 1.5 μm, and again coinciding with the detection of the silicon substrate, the amplitude of titanium becomes higher until the interface with the silicon is reached.

Noticeably, while the shape of the Ti peaks does not change in the depth profile, there is a change in the shape of the thinner Cr peaks right after the early detection of the silicon substrate at 1.5 μm. The Cr peaks become broader with a clear asymmetry that moves from the left to right side of the peak with the sputtering depth. In parallel, the Si rising tail shows in this region small oscillations coinciding with the Ti maxima. As discussed below, all these features arise as an outcome of the crater edge effects, with the result of dissimilar shapes for the Ti and Cr profiles as a consequence of the different sputtering rates of these layers. Furthermore, the possibility of simultaneous detection of two consecutive bilayers should not be disregarded, especially for the case of Cr showing larger profile tails after the interfaces with titanium.

Absolutely different profiles were obtained when we reversed the order of the multilayer components (10 bilayers of 70 nm titanium and 150 nm chromium). Fig. 4 shows the quantified GDOES depth profiles of such a system. It can clearly be observed how the peaks of the chromium layers slightly decrease down to a minimum of approximately 90% for the

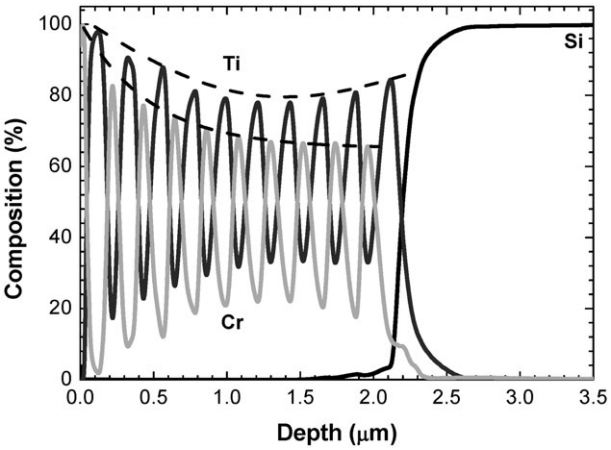

Fig. 2 GDOES depth quantified profile of the 10 × (70 nm chromium/150 nm titanium) multilayer coating on silicon. The broken lines follow the variation of the metal peak intensities with depth.

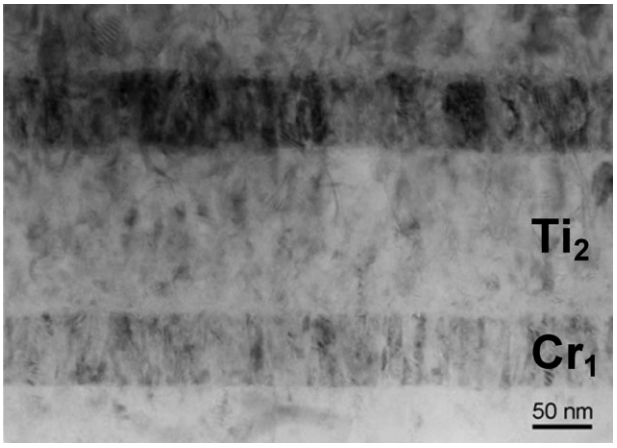

Fig. 1 Cross sectional TEM micrograph showing the periodical structure of the first layers of the 10 × (70 nm chromium/150 nm titanium) multilayer coating.

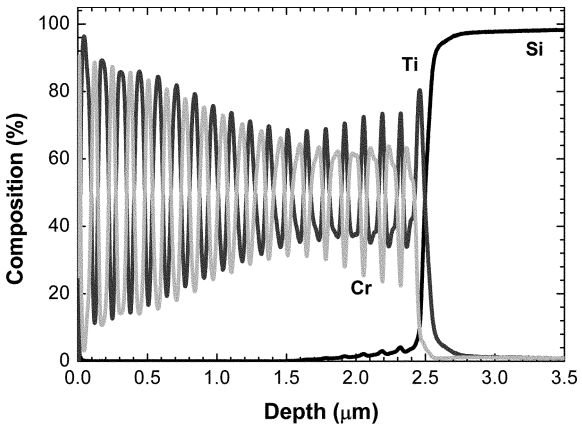

Fig. 3 GDOES depth quantified profile of the 20 × (55 nm chromium/70 nm titanium) multilayer coating on silicon.

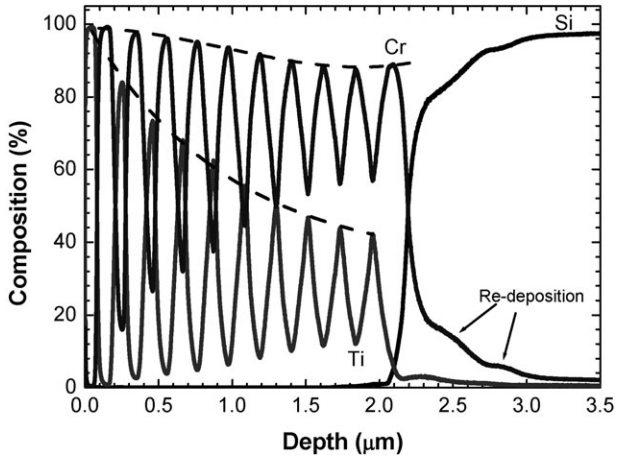

Fig. 4 GDOES depth quantified profile of the 10 × (70 nm titanium/150 nm chromium) multilayer coating on silicon. The broken lines follow the variation of the metal peak intensities with depth. The arrows indicate signal of re-deposited Cr material on the crater walls.

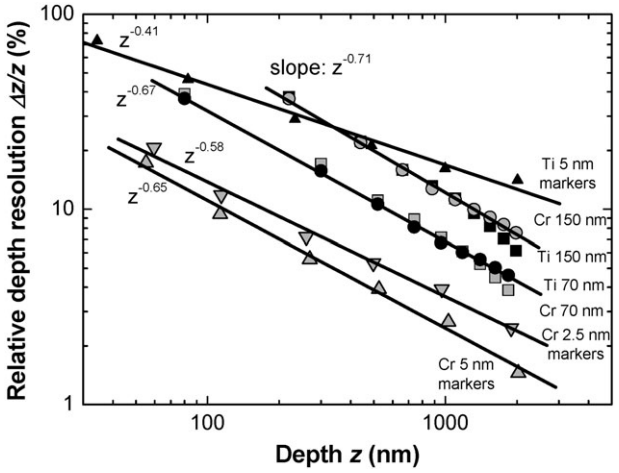

Fig. 5 Relative depth resolution dependence with depth (in logarithmic scale) of the metal interfaces present in the different multilayer systems and delta markers.

last layer. On the contrary, the titanium content rapidly degrades as the peaks are reduced to 40%, showing that there is more chromium than titanium content in the last four Ti layers!

The different behaviour observed for the multilayer coatings in Figs. 2 and 3 can be discussed again in terms of the SR of the Cr and Ti layers. As was mentioned above, the sputtering rate of chromium is more than 50% higher than those of titanium and silicon. Therefore, in the vicinity of the interface of two materials, the low sputtering rate component is more efficiently mixed with the other metal and, conversely, the high sputtering rate component is less degraded. Furthermore, the higher the sputtering rate, the deeper the crater edge. Hence, the sputtering of chromium affects more the titanium layers content than *vice versa*, producing a higher mixing of the Ti layers. This effect is enhanced in the case of Fig. 4, where the titanium layers are thinner than the chromium ones. Obviously, the mixing of the layers increases with depth, as the depth resolution is worsened by the roughness induced by the sputtering process. Shimizu *et al.*[15] pointed out that variations of sputtering rate across the crater mainly determine the degradation of depth resolution in GDOES. In that study such variations were a maximum of 6%.

This implies that the effects observed in our case, where the sputtering rate varies by a factor 1.5 in every bilayer period, will be much more severe.

Fig. 4 also gives a clear picture of the re-deposition effect on the crater walls, discussed in our previous paper for thicker layers. This is more apparent at the Si interface, where both the Cr and Ti signals penetrate about 1 μm deep after the Cr/Si interface, giving rise to a slow increase of the Si profile in that region. But, as consequence of the differences in the SR, the Cr signal penetrates further than the Ti one. In addition, the tails present a waving decay, showing at least two relative maxima in the Cr signal and, with less intensity, in the Ti one (see arrows in Fig. 4). This indicates that Cr and Ti material coming from the last two layers, and re-deposited on the crater walls, is still being sputtered. The contribution of the two metals after the Si interface in thin multilayer systems is in contrast to the results obtained for thicker multilayers, where only the adjacent metal is detected.[17]

We have calculated the depth resolution Δz of the different multilayers using formula (1). This expression relates the multilayer amplitudes (I_m), normalized to the intensity of the non-degraded layer (I_o), with the constant layer thickness, d, and the depth resolution, Δz.[20,21] Although the formula is valid only for a multilayer system A/B/A/B..., with the same layer thickness ($d_A = d_B = d$), we have applied it here as a first approximation to our multilayer system ($d_A \neq td_B$).

$$\frac{I_m}{I_o} = 2\left[\mathrm{erf}\left(\frac{d}{\sqrt{2}\Delta z}\right) - \mathrm{erf}\left(\frac{3d}{\sqrt{2}\Delta z}\right) + \mathrm{erf}\left(\frac{5d}{\sqrt{2}\Delta z}\right) \mp \ldots\right] - 1 \quad (1)$$

Using this formula, the relative depth resolution $\Delta z/z$, has been plotted in Fig. 5 (on a logarithmic scale) as a function of the interface depth z, for the different Cr and Ti layers of Figs. 2 and 4. It can be observed how there is practically the same dependence with depth ($\sim z^{-0.7}$) for all the layers, although the thicker 150 nm layers have a larger $\Delta z/z$. The 150 nm Ti and 70 nm Cr layers slightly deviate from this behaviour after a depth of approximately 1500 nm, corresponding to the early detection of the silicon substrate observed in Fig. 2. These results are in agreement with the work of other authors.[20]

(b) Evaluation of depth resolution function: Cr markers on Ti matrix

The analysis of thin anodic alumina films, with 2 nm thick Cr delta function marker layers, performed by Shimizu *et al.*,[10–15] is likely to be one of the most interesting studies on the evaluation of the GDOES depth resolution. We have intended to follow that work with a different approach, by depositing ultra-thin Cr markers at different depths in a titanium matrix. Such thin layers (approximately delta function layers) were used to evaluate the depth resolution function (DRF) of our system. As is known, the experimentally measured profile, represented by $C(x)$, can be expressed as a convolution of the real depth profile $T(x)$ and the DRF, $g(x - x')$, in the following way:

$$C(x) = \int_{-\infty}^{+\infty} T(x')g(x - x')\mathrm{d}x' \quad (2)$$

The DRF describes sputtering-induced effects that broaden the measured profile worsening the depth resolution. When the roughness is the main factor affecting the depth resolution, this DRF is predicted to be a Gaussian-like function.[20,21] Once the resolution function is known, then the true depth profile can be determined applying deconvolution procedures. This approach, widely used in SIMS and AES,[20] has been nicely described by Quentmeier in ref. 22. It is understood that such a DRF would only comprise roughening effects. Other degradation agents described above related to the crater shape (*i.e.*, re-deposition on the crater wall and crater edge well) are not included. In ref. 23 Weiss presents a model to include the crater effects assuming a DRF changing with depth.

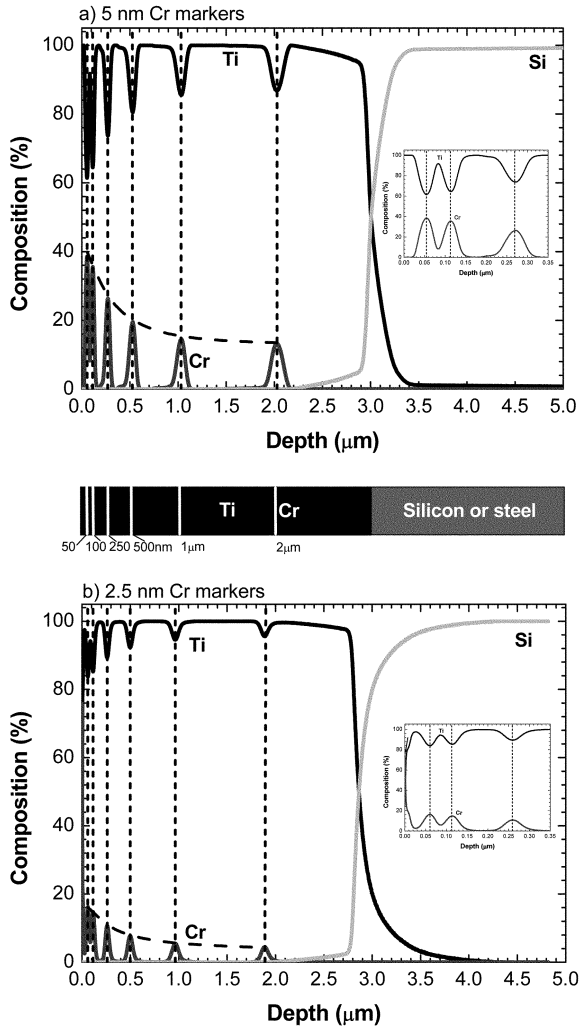

Fig. 6 GDOES depth quantified profile of the multilayer coating consisting of (a) 5 nm and (b) 2.5 nm Cr layers embedded in a Ti matrix deposited on silicon. The broken lines follow the variation of the chromium peak intensities with depth. The dotted vertical lines indicate the position of the markers. The inset graphs show a zoom in of the profiles down to the first 350 nm.

To this end, a multilayer system consisting of six layers of chromium (5 nm thick) buried in between titanium layers of variable thickness, were deposited on silicon and steel substrates. The total thickness of the coatings was measured by profilometry to be 3 μm. The Cr markers were deposited at depths of 0.05, 0.1, 0.25, 0.5, 1 and 2 μm from the coating surface. Fig. 6(a) shows the GDOES depth profile performed at 650 Pa and 40 W along with a scheme of the system studied (bottom panel).

The six 5 nm Cr markers are perfectly identified in the depth profile even when embedded a few microns deeper into the Ti matrix. Near the outmost surface (see the inset in Fig. 6(a)), the first two markers, although detected, were not well resolved because of their proximity (50 nm). The height of the Cr peaks decreases with depth (see broken line) while increasing their width. This reveals a loss in depth resolution during the GDOES experiment.

Using the approach given by Hofmann[20] for the case of a thin sandwich layer of thickness d, we have calculated depth resolution Δz through the formula (3) which relates the decrease of the peak intensity (ideally I_o) to a value I_s with Δz.

$$\frac{I_s}{I_o} = \mathrm{erf}\left(\frac{d}{\sqrt{2}\Delta z}\right) \qquad (3)$$

The results for the relative depth resolution of the Cr markers have been plotted in Fig. 5 as a function of depth. Note that the relative depth resolution shows a dependence of the type $z^{-0.65}$.

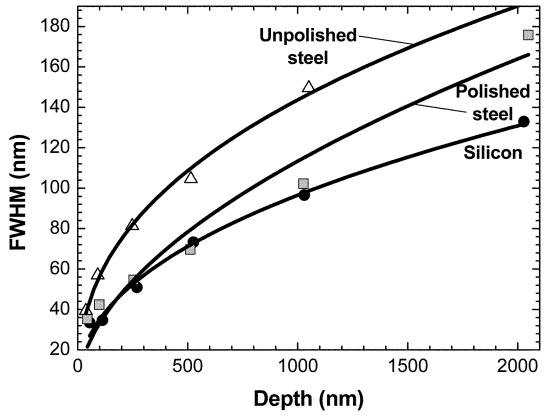

Fig. 7 Relationship of the full width half maximum of the 5 nm Cr markers peaks with the depth for samples deposited on silicon (closed circles), polished steel (grey squares) and unpolished steel (open triangles). The solid lines represent power law fits ($y = ax^b$) of the experimental data.

In order to obtain the DRF, a Gaussian fit of the peaks was carried out. The excellent agreement of the fit to the experimental data ($r^2 = 0.995$) confirms that the loss in depth resolution at the interfaces is mainly due to a roughness increase during the GDOES experiment (exception made of the other edge effects reflected by the profile tails, not considered in this approach). In Fig. 7, the dependence of the full width at half maximum (FWHM) of the fitted peaks is plotted *versus* depth, for samples deposited on three different substrates: silicon, and polished and unpolished steel. Using a power law relation ($y = ax^b$, with $b = 0.44 \pm 0.02$) a very good fit of the FWHM of the Cr marker with the depth was found in the case of the silicon substrate. The exponent value b obtained is very close to the square-root dependence ($b = 0.5$) expected from Gaussian resolution functions.[20] Therefore, we have used this Gaussian function, with a FWHM varying in depth, as the resolution function of our system. First attempts using simple Van Cittert[24] and Gold[25–27] deconvolution algorithms resulted in an improvement of the resolution of the Cr peaks. As an example, the first two Cr peaks can be now properly resolved. These results will be extended in a later work.[28]

Further experiments using thinner 2.5 nm Cr markers were also made under the same conditions. An additional marker was deposited at the outmost surface of the coating. Fig. 6(b) shows how the seven markers were again detected although their intensities are much lower. The first marker at the outmost surface is clearly observed (see inset graph in Fig. 6(b)), with an intensity of approximately 80%. The intensity of the following peak at 50 nm decreases dramatically to a value lower than 20%. The relative depth resolution of the 2.5 nm peaks was found to have a $z^{-0.58}$ dependence with depth, as shown in Fig. 5. These experiments show the excellent capabilities of the rf-GDOES technique to detect buried thin films and interfaces in the nanometre range (below 2.5 nm).

Finally, in order to check the effect of the differences of the SR between the elements of the multilayer system, we deposited seven 5 nm titanium markers on a chromium matrix at the same depths as in Fig. 6. Apart from the broader Si interface, already discussed, it can also be observed in Fig. 8 that the degradation of the Ti markers is much more severe than for the chromium case of Fig. 6(a). Applying again eqn. (3) a higher depth resolution was found (*i.e.*, 6 times larger at 1.0 μm). The relative depth resolution of the 5 nm Ti markers has a $z^{-0.41}$ dependence with depth, as shown in Fig. 5.

As a conclusion, we can state that GDOES experiments have been found to properly reproduce the period and thickness of different Cr and Ti thin (<150 nm) and ultrathin (<10 nm) multilayer systems. However, we have observed a degradation

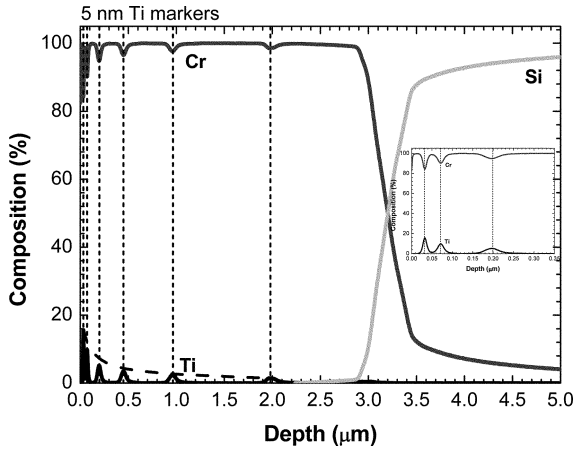

Fig. 8 GDOES depth quantified profile of the multilayer coating consisting of 5 nm Ti layers embedded in a Cr matrix deposited on silicon. The broken lines follow the variation of the chromium peak intensities with depth. The dotted vertical lines indicate the positions of the markers. The inset graph shows zoom in of the profile down to the first 350 nm.

of the original concentration profiles. The effect of the crater effects factors, previously reported, is more apparent when the thicknesses of the individual multilayers approach, or are narrower than, the rising and decaying tails of the corresponding profiles observed in thicker films. For such narrow films, the continuous change in the crater shape after each interface further enhances the mixing of the layers. The profile degradation has been found to be dependent on the sputtering rate of the materials as well as on the interface depth. The depth resolution function of the system was evaluated using ultrathin (2.5 and 5 nm) chromium delta markers. A Gaussian fit of the markers confirmed the roughness-limited nature of the GDOES depth resolution. These experiments demonstrate the excellent capabilities of the rf-GDOES technique to detect thin films in the nanometre range.

Acknowledgements

The authors wish to thank N. J. M. Carvalho (University of Groningen) for the cross-sectional TEM micrograph.

References

1 *Glow Discharge Optical Emission Spectrometry*, eds. R. Payling, D. Jones and A. Bengtson, John Wiley & Sons, New York, 1997, ch. 7.
2 M. R. Winchester and R. Payling, *Spectrochim. Acta, Part B*, 2004, **59**, 607.
3 J. Angeli, A. Bengston, A. Bogaerts, V. Hoffmann, V. Hodoroaba and E. Steers, *J. Anal. At. Spectrom.*, 2003, **18**, 670.
4 S. Oswald and S. Baunack, *Thin Solid Films*, 2003, **425**, 9.
5 V. Hodoroaba, W. E. S. Unger, H. Jenett, V. Hoffmann, B. Hagenhoff, S. Kayser and K. Wetzig, *Appl. Surf. Sci.*, 2001, **179**, 30.
6 J. A. García, R. J. Rodríguez, R. Martínez, C. Fernández, A. Fernández and R. Payling, *Appl. Surf. Sci.*, 2004, **235**, 97.
7 A. Thobor, C. Rousselot and S. Mikhailov, *Surf. Coat. Technol.*, 2003, **174–175**, 351.
8 S. Hofmann, *J. Vac. Soc. Jpn.*, 1990, **33**, 721.
9 S. Hofmann and K. Yoshiharam, *J. Surf. Anal.*, 1990, **21**, 673.
10 K. Shimizu, G. M. Brown, H. Habazaki, K. Kobayashi, P. Skeldon, G. E. Thompson and G. C. Wood, *Surf. Interf. Anal.*, 1999, **27**, 24.
11 K. Shimizu, G. M. Brown, H. Habazaki, K. Kobayashi, P. Skeldon, G. E. Thompson and G. C. Wood, *Electrochim. Acta*, 1999, **44**, 2297.
12 K. Shimizu, H. Habazaki, P. Skeldon, G. E. Thompson and G. C. Wood, *Surf. Interf. Anal.*, 2000, **29**, 155.
13 K. Shimizu, H. Habazaki, P. Skeldon and G. E. Thompson, *Spectrochimica Acta, Part B*, 2003, **58**, 1573.
14 K. Shimizu, H. Habazaki, P. Skeldon and G. E. Thompson, *Surf. Interf. Anal.*, 2003, **35**, 564.
15 K. Shimizu, H. Habazaki, P. Skeldon, G. E. Thompson and R. K. Marcus, *Surf. Interf. Anal.*, 2001, **31**, 869.
16 V. Hoffmann, R. Dorka, L. Wilken, V. D. Hodoroaba and K. Wetzig, *Surf. Interf. Anal.*, 2003, **35**, 575.
17 R. Escobar Galindo, E. Forniés and J. M. Albella, *J. Anal. At. Spectrom.*, 2005, DOI: 10.1039/b502771c.
18 M. A. Auger, R. Gago, M. Fernández, O. Sánchez and J. M. Albella, *Surf. Coat. Technol.*, 2002, **157**, 26.
19 A. Quentmeier, in *Glow Discharge Optical Emission Spectroscopy*, eds. R. Payling, D. G. Jones and A. Bengston, John Wiley & Sons, 1997, Sections 7.1 and 7.2.
20 S. Hofmann, in *"Practical Surface Analysis by Auger and X-ray Photoelectron Spectroscopy"*, eds. D. Briggs and M. P. Seah, John Wiley & Sons, 1983, ch. 4.
21 S. Hofmann, *Surf. Interf. Anal.*, 1999, **27**, 825.
22 A. Quentmeier in *Glow Discharge Optical Emission Spectroscopy*, eds. R. Payling, D. G. Jones and A. Bengston, John Wiley & Sons, 1997, Section 7.3.
23 Z. Weiss in *Glow Discharge Optical Emission Spectroscopy*, eds. R. Payling, D. G. Jones and A. Bengston, John Wiley & Sons, 1997, Section 7.5.
24 P. H. Van Cittert, *Z. Phys.*, 1931, **69**, 298.
25 R. Gold, ANL-6984, Argonne National Laboratories, Argonne, 1964.
26 P. Bandžuch, M. Morháč and J. Krištiak, *Nucl. Instrum. Meth. Phys. Res. A*, 1997, **384**, 506.
27 M. Morháč, J. Kliman, V. Matoušek, M. Veselský and I. Turzo, *Nucl. Instrum. Meth. Phys. Res. A*, 1997, **401**, 385.
28 R. Escobar Galindo, C. Palacio and J. M. Albella, 2004, to be published.